JOURNAL OF AIRCRAFT
Vol. 41, No. 5, September–October 2004

Interdependence of Diffusion and Straining of Helicopter Blade Tip Vortices

Manikandan Ramasamy* and J. Gordon Leishman†
University of Maryland, College Park, Maryland 20742

An experiment was performed to help quantify the interdependence of viscous/turbulent diffusion and straining effects on the development of helicopter rotor tip vortices. The properties of the blade tip vortices were measured in the wake of a small-scale hovering rotor and compared to the results for the case when the wake approached a solid boundary. The presence of the boundary created velocity gradients that forced the tip vortex filaments to strain, allowing the effects of this process on the vortices to be measured relative to the baseline case without the boundary. It is shown that vortex stretching begins to decrease the viscous core size, and when the strain rates become large, this can balance the normal growth in the vortex core resulting from diffusion. The present results were used to help develop a more general tip vortex model suitable for use in a variety of helicopter rotor aeroacoustic applications. The proposed engineering model combines the effects of turbulent diffusion and strain on the vortex core growth. The empirical coefficients of this model have been derived based on the best available results from rotating-wing tip vortex measurements.

Nomenclature

A	=	rotor disk area, πR^2, m^2
a_1	=	Squire's coefficient
C_T	=	rotor thrust coefficient, $T/(\rho A \Omega^2 R^2)$
c	=	rotor blade chord, m
$\bar{d}$	=	nondimensional downstream distance
e	=	correlation coefficient
k	=	empirical constant
l	=	filament length, m
p	=	probability density function
R	=	rotor radius, m
Re_v	=	vortex Reynolds number, Γ_v/ν
r	=	radial distance, m
r_c	=	viscous core radius, m
$\boldsymbol{r}_l$	=	position vector of the filament, m
r_p, z_p	=	laser Doppler velocimetry measurement location with respect to rotor axes
r_v, z_v	=	vortex core location with respect to rotor axes
r_0	=	initial core radius, m
$\bar{r}$	=	nondimensional radial distance, r/r_c
T	=	rotor thrust, N
t	=	time, s
V_ε	=	filament strain rate, ms^{-1}
V_θ	=	swirl velocity, ms^{-1}
V_∞	=	freestream velocity, ms^{-1}
z	=	downstream distance, m
α	=	Oseen constant, 1.25643
Γ_v	=	tip vortex strength (circulation), m^{2}s^{-1}
δ	=	effective diffusion constant
ε	=	filament strain
ζ	=	wake (vortex) age, deg
ν	=	kinematic viscosity, m^{2}s^{-1}
ρ	=	flow density, kg m^{-3}
σ_r, σ_z	=	standard deviation of vortex location in radial and axial directions, respectively, m
ψ	=	azimuth angle, deg
Ω	=	rotor rotational speed, rad s^{-1}
$\boldsymbol{\omega}$	=	vorticity, m^{2}s^{-1}

Received 25 June 2003; revision received 9 July 2003; accepted for publication 27 July 2003.

*Graduate Research Assistant, Department of Aerospace Engineering, Glenn L. Martin Institute of Technology; mani@glue.umd.edu.

†Professor, Department of Aerospace Engineering, Glenn L. Martin Institute of Technology; leishman@eng.umd.edu.

Introduction

CONSIDERABLE prior research has been conducted into the problem of measuring the development of blade tip vortices trailed into the wakes of helicopter rotors. The structure of the tip vortices define the majority of the induced velocity field at the rotor, as well as being responsible for a number of adverse problems, including unsteady blade airloads and high rotor noise levels associated with blade vortex interactions (BVI). Therefore, better models of the tip vortex structure should, in principle, translate directly into improved predictions of the unsteady airloads on the blades, better predictions of rotor vibration levels, and also in a more complete understanding and predictive capability for BVI noise.

The reduction of helicopter rotor noise has become an important goal from both military and civilian perspectives. Small changes in the structure of the tip vortices (such as their core size) and their spatial positions relative to the rotor blades can have substantial effects on BVI noise.[1] The blades may also interact with vortex filaments that are relatively old, which means that the filaments need to be modeled accurately at large wake ages (in terms of rotor revolutions). During this time, the vortex filaments will have undergone some amount of viscous and turbulent diffusion (depending on the vortex Reynolds number), as well as encountering the steep velocity gradients inside the rotor wake that also must affect their evolution. This suggests that vortex models need to be developed with relatively high levels of fidelity to ensure sufficient confidence levels in the unsteady airloads and noise predictions. Only then can effective strategies aimed at rotor noise control or the alleviation of other adverse vortex-induced phenomena be properly considered.

There has been much experimental work done in an attempt to measure and otherwise characterize the structures of helicopter blade tip vortices. A good summary of the numerous experiments, as well as the relative capabilities, limitations, uncertainties, and precision of the different measurement techniques is given by Martin et al.[2] Typical experimental goals include the measurement of the induced velocity field close to the vortex axis, the net vortex strengths, the size of the viscous core, and the rate of growth of the core as the tip vortex advects and ages in the downstream wake. However, making measurements of the tip vortices generated by rotating blades is very challenging.[3] Unlike fixed wings, which trail rectilinear

vortices, helicopter tip vortices are curved and also lie in proximity to other vortices, producing both self- and mutually-induced induction effects on their development.

Another complication is that the blade tip vortices also experience strain effects as they are advected in the steep velocity gradients produced inside the rotor wake, especially when the helicopter is in forward flight or during descent. This means that filaments must undergo continuous changes in their vorticity field, even in the absence of ongoing diffusion.[4] Such straining effects have also been shown significant in other problems in fluid mechanics.[5] Straining produces additional effects on the local velocity field induced by the tip vortices, and so this impacts the development of the overall wake as adjacent vortex segments move relative to each other. As shown by Ananthan et al.,[6] this can be a modeling issue for helicopter rotors in forward flight, where individual vortices tend to bundle and roll up tightly together from the lateral edges of the rotor disk. These straining effects can also make the measured vortex properties different from those that might be obtained with equivalent rectilinear (fixed-wing) vortices, which develop in a more benign flow environment, although they also may be subjected to induction effects. Therefore, isolating the various contributing effects is essential for the development of better tip vortex models for use in helicopter rotor applications.

In addition to the practical difficulties in making rotor flow and tip vortex measurements and isolating several interdependent physical effects, another concern is that the measurements must usually be made on subscale rotors. This is a situation of necessity because of the enormous practical difficulties and huge costs in making measurements with the necessary fidelity on full-scale rotors. However, amongst other issues, this raises questions about flow scaling effects, which at model scale may have vortex Reynolds numbers that may be up to two orders of magnitude less than those associated with full-scale rotors. The vortex Reynolds number is known to affect both the structure and the viscous growth rate of the tip vortices (see Refs. 7–11), although the dearth of measurements over a sufficiently wide range of vortex Reynolds number means that this dependency has not yet been fully quantified.

The present work has two goals. First is to perform an idealized experiment in an attempt to examine any interdependence of straining and viscous/turbulent diffusion on the development of helicopter rotor tip vortices. Vortex properties were compared to results for the case when the rotor wake was advected toward a solid boundary. The presence of the boundary forced the tip vortices to stretch in a known (estimated) strain field, allowing the effects to be measured and isolated. Second is to reexamine the issues of vortex modeling, from the practical perspective of including such models in comprehensive rotor simulations,[12–14] with the objective of improving the fidelity of the modeling. Problems considered herein include the modeling of viscous/turbulent diffusion, the interdependent modeling of strain effects, and the issues of vortex Reynolds number scaling.

Description of the Experiment

Rotor Facility

A single-bladed rotor operated in the hovering state was used for the flow measurements. The blade was of rectangular planform, untwisted, with a radius of 406 mm (16 in.) and chord of 44.5 mm (1.752 in.), and was balanced with a counterweight. The blade airfoil section was the NACA 2415 throughout. The rotor tip speed was 89.28 m/s (292.91 ft/s), giving a tip Mach number and chord Reynolds number of 0.26 and 2.72×10^5, respectively. The advantages of the single-bladed rotor have been addressed before.[15,16] This includes the ability to create and study a helicoidal vortex filament without the interference from the other vortices that would be generated by other blades.[15] Furthermore, a single helicoidal vortex is much more spatially and temporally stable than a set of interdigitated vortices.[16] This allows the vortex structure to be studied at much older wake ages and also relatively free of the large flow aperiodicity issues that affect multibladed rotor experiments.

All of the tests were made at an effective blade loading of $C_T/\sigma \approx 0.064$ using a collective pitch of 4.5 deg (measured from the chord line). The zero lift angle of attack of the NACA 2415 is approximately -2 deg. During these tests, the rotor rotational frequency was set to 35 Hz ($\Omega = 70\pi$ rad/s). The rotor was tested in the hovering state in a flow conditioned test cell. The volume of the test cell was approximately 362 m^3 (12,800 ft^3) and was surrounded by honeycomb flow conditioning screens. This cell was located inside a large 14,000 m^3 (500,000 ft^3) high-bay laboratory. In the baseline case, the wake was allowed to exhaust approximately 18 rotor radii before encountering flow diverters. Aperiodicity levels in the rotor wake have been measured and were used to correct the velocity field measurements; see the Appendix.

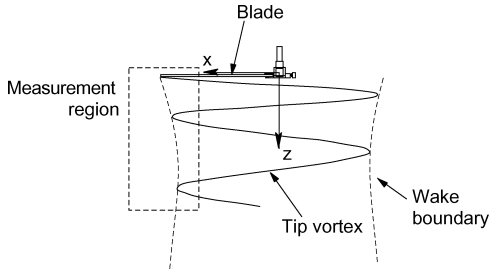

a) Baseline configuration, rotor operates in free air

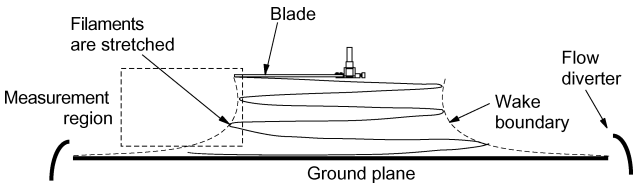

b) Rotor operates next to ground plane

Fig. 1 Schematic showing the experimental setup.

Ground Plane

To examine the effects of superimposed velocity gradients on the tip vortex developments, an artificial means was developed using a solid boundary or ground plane. Based on the experiments of Light and Norman,[17] tip vortex strain calculations showed that significant values could be expected. A schematic of the present experimental setup is shown in Fig. 1. The ground plane was twice the rotor diameter and could be adjusted to obtain different distances from the rotor plane. For the present tests, the distance was set to $0.5R$. As the rotor wake approached this ground plane, the vortex filaments were rapidly strained in the radial direction away from the rotor. The present measurements were made at up to $0.05R$ from the ground plane.

The possibilities of aperiodicity and recirculation of the wake was reduced by the use of a flow diverter placed around the circumference of the ground plane. This directed the rotor wake to flow behind the ground plane. A further series of flow diverters behind the plane was used to control the overall flow quality, which was verified using flow visualization. The inherent difficulties in measuring vortex-induced velocities close to surfaces, and also in measuring the velocity profiles of tip vortices at older wake ages, however, imposed restrictions on how close the plane could actually be placed to the rotor.

Flow Visualization

Flow visualization images were acquired by seeding the flow using a mineral oil fog strobed with a laser sheet. The light sheet was produced by a dual Nd:YAG laser. The light sheet was located in the flow using an optical arm. Images were acquired using a charge-coupled device (CCD) camera and were later digitized using a particle image velocimetry-type calibration grid. The laser and the camera were synchronized using electronics that converted the rotor one-per-revolution frequency trigger into a signal that pulsed every third rotor revolution. A phase delay was introduced so that the laser could be fired at any rotor phase (blade azimuth) angle.

The seed was produced by vaporizing a mineral oil into a dense fog. The oil was broken down into a fine mist by adding nitrogen under pressure, forced into a heater block, and heated to its boiling point, where it became vaporized. As the vapor escaped from the heat exchanger nozzle, it was mixed with ambient air, rapidly cooled, and condensed into a fog. From a calibration, 95% of the particles were between 0.2 and 0.22 μm in diameter. This mean seed particle size was small enough to minimize particle tracking errors for the vortex strengths found in these experiments.[18] The fog/air mixture was passed through a series of ducts and introduced into the rotor flowfield at various strategic locations.

Laser Doppler Velocimetry System

A fiber-optic-based laser Doppler Velocimetry (LDV) system was used to make three-component velocity measurements. A beam splitter separated a single 6-W multi-line argon-ion laser beam into three pairs of beams (green, blue, and violet), each of which measured a single component of velocity. A Bragg cell, set to a frequency shift of 40 MHz, produced the second shifted beam of each beam pair. The laser beams were passed to the transmitting optics by a set of fiber-optic couplers with single-mode polarization preserving fiber-optic cables. The transmitting optics were located adjacent to the rotor (Fig. 2) and consisted of a pair of fiber-optic probes with integral receiving optics, one probe for the green and blue pairs and the other probe for the violet pair. Beam expanders with focusing lenses of 750 mm were used to increase the beam crossing angles and so to decrease the effective measurement volume.

To further reduce the effective size of the probe volume visible to the receiving optics, the off-axis backscatter technique was used, as described by Martin et al.[2] and Barrett and Swales.[19] This technique spatially filers the effective length of the LDV probe volume on all three channels. Spatial coincidence of the three probe volumes (all six beams) and two receiving fibers was ensured to within ± 15 μm by measuring the beam profiles and their spatial locations.[2] Alignment is critical for three-component LDV systems because it is geometric coincidence that determines the spatial resolution of the LDV probe volume. In the present case, the resulting LDV probe volume was measured to be an ellipsoid of dimensions 81 ± 6 μm by 145 ± 10 μm, which for reference was about 3% of the maximum blade thickness or 0.5% of the blade chord.

The high capacity of the seeder allowed the entire test cell to be uniformly seeded in approximately 30 s. Signal bursts from seed particles passing through the measurement volume were received by the optics and transmitted to a set of photomultiplier tubes, where they were converted to analog signals. This analog signal was low-bandpass filtered to remove the signal pedestal and any high-frequency noise. The large range of the low-bandpass filter was required to allow measurement of the flow reversal associated with the advection of a vortex core across the measurement grids. The analog signal was digitized and sampled using a digital burst correlator. The flow velocities were then converted into three orthogonal components based on measurements of the laser beam crossing angles. Each measurement was phase resolved with respect to the rotating blade by using a rotary encoder, which tagged each data point with a time stamp. The temporal phase resolution of the encoder was 0.1 deg, but the measurements were averaged into 1-deg bins. The uncertainty in this process has been discussed by Martin et al.[2]

Experimental Results

Wake Displacements and Strains

The strain rates acting on the tip vortices were determined based on measurements of the spatial locations of the vortex cores at various wake ages. To do this, flow visualization images were acquired at several wake ages using the strobed laser sheet technique. To make these images, the volume and distribution of seeding were judiciously adjusted so that the core region of the vortices appeared as distinct voids of seed. These seed voids were then used to estimate the centers of the vortex cores. At each wake age, a minimum of 300 separate images were taken, from which the spatial average locations of the vortex core relative to the rotor were quantified by using a calibration grid. These locations were also cross checked against the velocity field measurements using the LDV system. The flow visualization results were further used to acquire statistics of the small aperiodic deviations of the vortex positions from their mean position at a given wake age and were used to correct the LDV measurements for these effects (see the Appendix).

From the results shown in Figs. 3 and 4, it is apparent that at early wake ages the tip vortices move inboard radially from the blade tip and axially downward. In both cases, the axial advection velocities were, as expected, nominally constant until the first blade passage at $\zeta = 360$ deg. Because of the ground plane, the tip vortices then started to move radially outward and became almost parallel to the ground plane at older wake ages. It can be deduced from Fig. 4

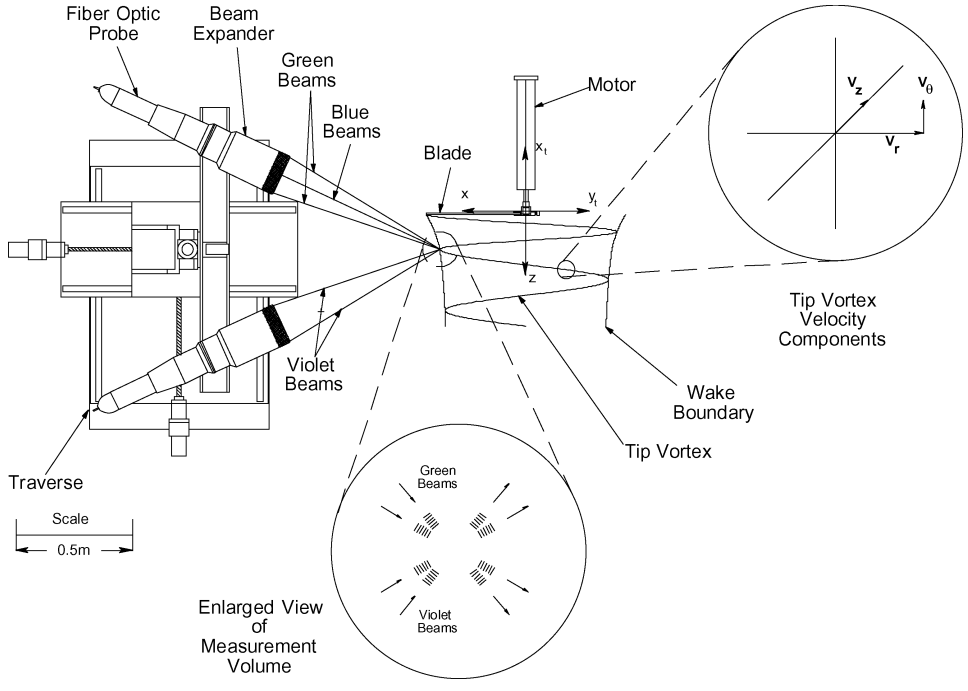

Fig. 2 Setup of three-component LDV system.

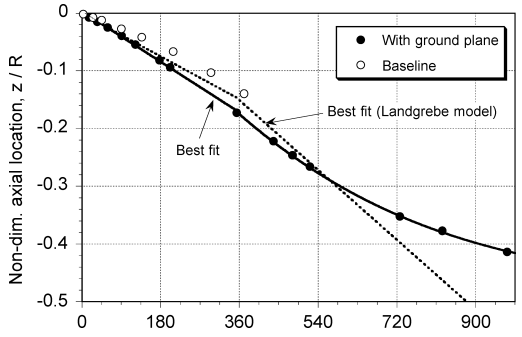

a) Axial displacements

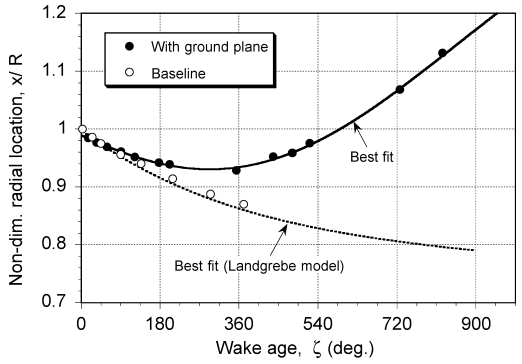

b) Radial displacements

Fig. 3 Results showing the axial and radial locations of the tip vortices relative to the rotor tip path plane.

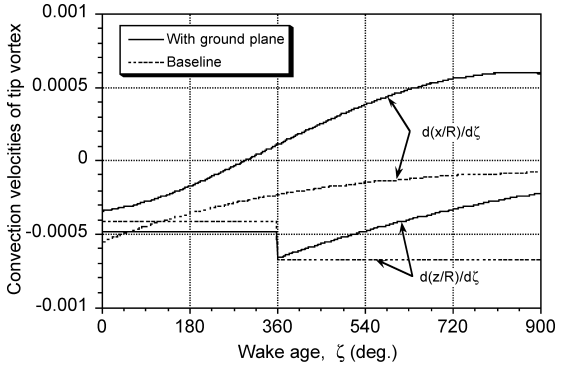

Fig. 4 Estimated components of the tip vortex advection velocities compared to the baseline condition.

that the tip vortices advect through the flow at a modest rate at early wake ages, but encounter much higher overall flow velocities when in closer proximity to the ground plane. Clearly, the axial (slipstream) advection velocity of the tip vortices asymptote to zero as they approach the ground plane.

After the spatial locations of the tip vortices were measured, the average strain rates acting on the vortex filaments was calculated numerically. From the locations of the vortices at various wake ages, the length of the vortex filament was determined by its location in space as defined by the position vectors of two adjacent locations at $\boldsymbol{r}_l$ and $\boldsymbol{r}_{l-1}$. If the filament is assumed to be a small straight-line segment, the length of the filament is given by $|\boldsymbol{l}| = |\boldsymbol{r}_l - \boldsymbol{r}_{l-1}|$. Therefore, the rate of change of the length of the filament as it advects through the velocity field is given by

$$\frac{\mathrm{d}\boldsymbol{l}}{\mathrm{d}t} = \frac{\mathrm{d}(\boldsymbol{r}_l - \boldsymbol{r}_{l-1})}{\mathrm{d}t} \tag{1}$$

or

$$\frac{\mathrm{d}\varepsilon}{\mathrm{d}t} = \frac{\mathrm{d}l}{\mathrm{d}t}\left(\frac{1}{l}\right) \tag{2}$$

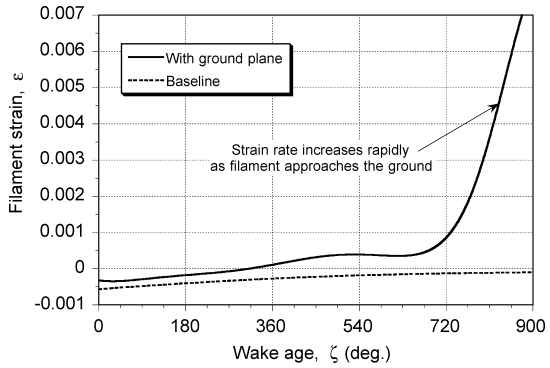

Fig. 5 Estimated strain experienced by the vortex filaments as they approach the ground plane compared to the baseline condition.

which implies that the strain ε is

$$\varepsilon = \left(\frac{\mathrm{d}\varepsilon}{\mathrm{d}t}\right)\Delta t = \left(\frac{\mathrm{d}\varepsilon}{\mathrm{d}\zeta}\right)\Delta\zeta \tag{3}$$

where $\varepsilon = \Delta l / l$ is the strain imposed on the filament over the time interval Δt.

Results documenting the measured strains are shown in Fig. 5. Notice that the amount of strain produced on the tip vortex as it develops near the ground plane is much larger than that obtained in the baseline case at equivalent ages without the plane. For the baseline case, the filament strain is negligible at older wake ages. This is expected because the results in Fig. 3 have shown that the radial locations of the tip vortices in this case begin to asymptote to a constant value, and the radial velocities approach zero after the initial wake contraction. When the tip vortices approach the ground plane, the strain on the tip vortex is initially slightly negative at early wake ages, which is similar to that found in the baseline case. Thereafter, the strain becomes quickly positive as the vortex filaments stretch radially outward in the steeper velocity gradients found near the plane.

Velocity Field Measurements

Phase-resolved LDV measurements of the vortex properties were acquired by making a radial traverse across the vortex core region over various planes inside the wake region between the rotor and the ground plane. When the blade azimuth at which the advecting vortex core was centered on the grid (wake age) is estimated, the instantaneous velocity field could be measured. Through postprocessing of the data, the tip vortex properties could be examined as a function of wake age. Wherever possible, the results measured with the ground plane were compared to the baseline measurements when at the same wake age. The ability to measure results at older wake ages ($\zeta > 360$ deg) is a result of both the stretching of the filaments and of the more precise spatial alignment of the LDV system.[2]

Swirl Velocities

Figure 6 shows a series of tangential (swirl) velocity profiles measured across each radial grid as the advecting vortices intersected the measurement grid in a crossflow plane (Fig. 1). These profiles are given in terms of the nondimensional distance with respect to a coordinate system centered at the vortex axis, and the velocity is nondimensionalized with respect to the rotor tip speed ΩR; in other words, all of the data are placed in a frame of reference moving along with the vortex. Furthermore, all of the data were corrected for the measured effects of aperiodicity (see the Appendix). Notice that the results in Fig. 6 show that peak swirl velocity decreases as the vortex ages, which is symptomatic of the effects of diffusion.

The distance between the peaks in each swirl velocity profile can be considered as the viscous core diameter (discussed later). The vortex core radius was determined from the LDV measurements based on a measurement of half the distance between two swirl velocity peaks. This determination was based on a spline curve fit

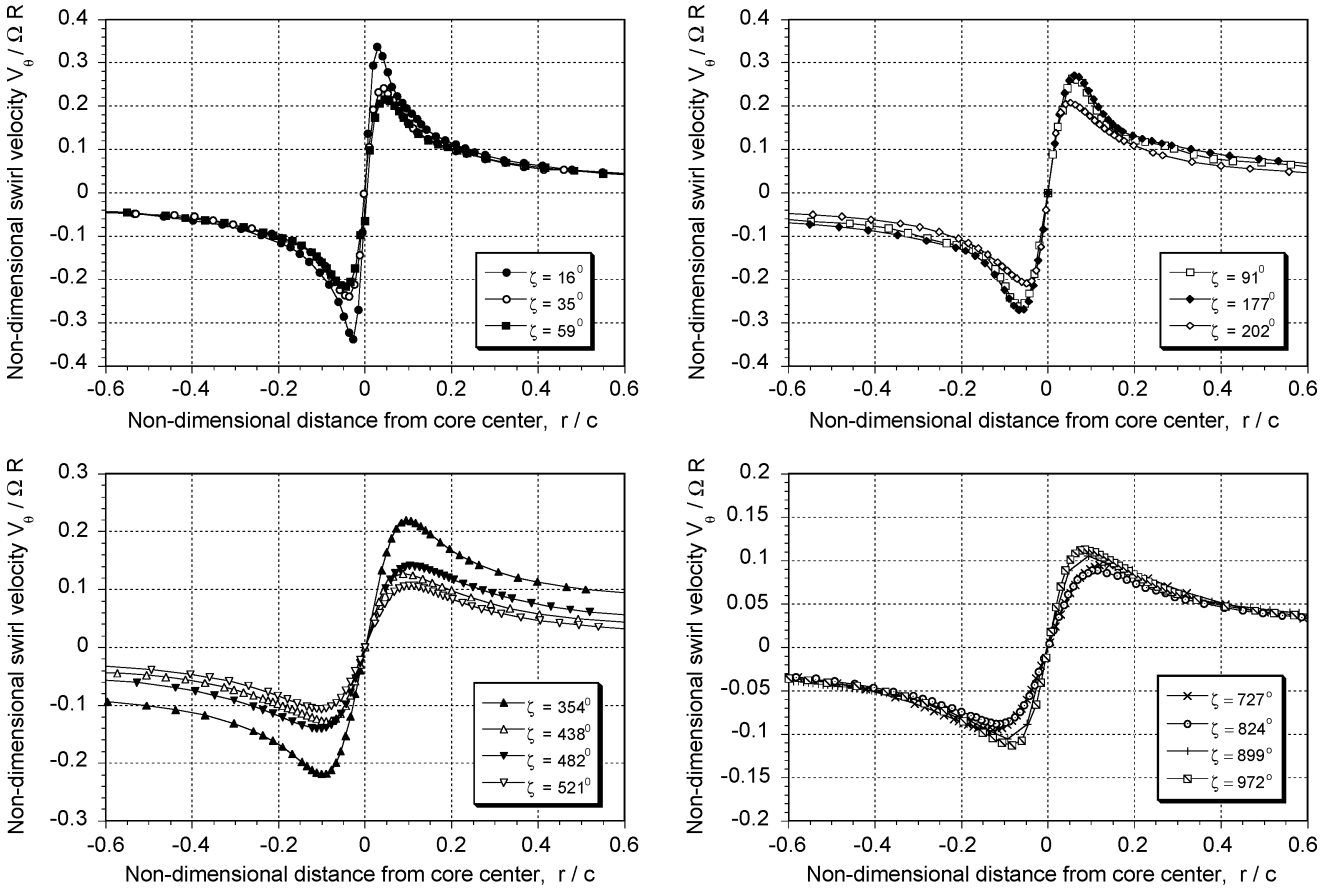

Fig. 6 Swirl velocity profiles in the tip vortex at different wake ages, showing the vortex diffuses under the action of viscosity.

to the measured velocity profiles, which was then used to find the distance between the two peaks. This technique helps remove the otherwise subjective nature of this determination process.

The peak swirl velocity at the earliest wake age ($\zeta = 16$ deg) was found to be about 35% of the tip speed and is typical of the values measured on helicopter rotors. The initial core radius was only 3.2% of blade chord (dimensionally, only 1.4 mm for this rotor), which gives some idea as the spatial resolution and alignment accuracy of the LDV system that is necessary to resolve the vortex core dimension. For the initial 600 deg of wake age, the strain rates are small (Fig. 4), and the vortex develops (diffuses) in a manner similar to that of the baseline case.[20] However, the last four measurements at $\zeta = 727$, 824, 899, and 972 deg clearly show a notable decrease in the core dimension, which is accompanied by a corresponding increase in the peak swirl velocity. This is now a clear reversal of the earlier trends, which suggests that the imposed strain rates had now affected the characteristics of the vortex. Measurements at wake ages older than 1000 deg were not possible because the tip vortices came too close to the ground plane to be able to exclude the consideration of external viscous effects.

Viscous Core Dimension

The deduced vortex core radius is plotted in Fig. 7 with respect to wake age. Figure 7 when compared along with Fig. 5, throws some light on the physics involved as the tip vortex is strained as it approaches the ground plane. At early wake ages, the two sets of results in Fig. 7 agree well, but with the presence of the ground plane, the core growth was found to be initially slightly larger. This reflects the initially lower (less positive) strain rate in the baseline case. More important, however, at later wake ages, the growth trend was found to be reversed as the strain rates became positive. These results suggest that the effects associated with straining begins to balance the normal core growth associated with viscous/turbulent diffusion. At the older wake ages (near the ground), the filament

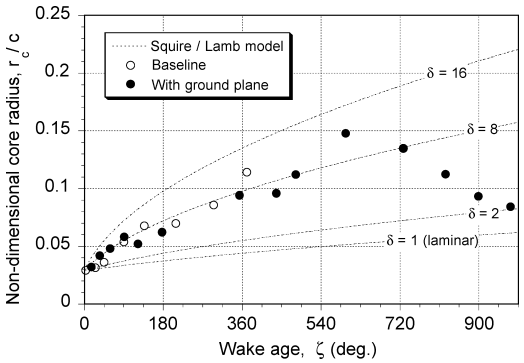

Fig. 7 Measured growth of the vortex core radius as a function of wake age.

starts to stretch at a much faster rate, as shown in Fig. 5, and this was noted to arrest distinctly the core growth. Results from the modified Squire[7]/Lamb[21]–Oseen[22] core growth model (also see Ref. 11) are also shown in Fig. 7, which are taken as a reference to represent the effects of diffusion on the core growth (discussed later). It is apparent that at earlier wake ages, the measured results follow this model quite well.

Circulation

The vortex circulation can be estimated from the measured swirl velocity distributions shown in Fig. 6, the results being shown in Fig. 8. The net circulation was determined at a distance of $0.25c$ from the vortex axis and by assuming flow axisymmetry in the reference system moving with the vortex core. The core circulation is that value contained within the dimension of estimated core radius. Notice that the values of net circulation decrease only relatively

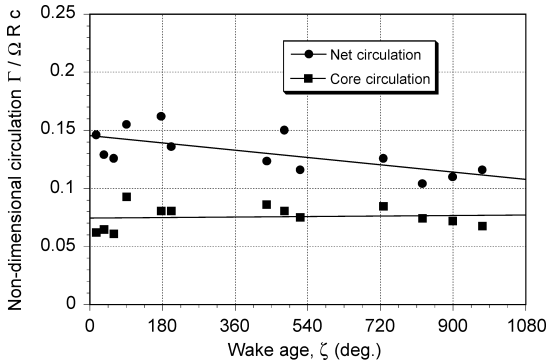

Fig. 8 Measured circulation as a function of wake age.

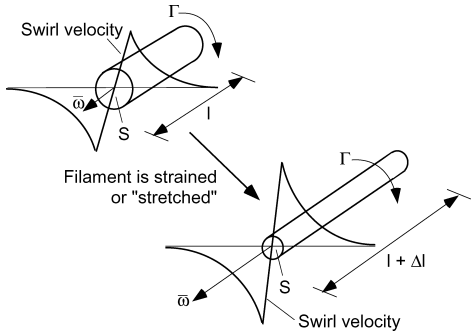

Fig. 9 Schematic showing the positive straining or stretching of a rectilinear vortex filament.

slowly with wake age, and the core circulation stays essentially constant. This confirms that dissipation of the vortex energy is small and that the competing mechanisms in the dynamics of the tip vortex evolution in this case are diffusion and strain, respectively.

Analysis and Discussion

Modeling of Diffusion

When presented in an axis system moving with the vortex core, the swirl velocity field induced by the trailing vortex resembles that of a potential vortex at a large distance from the vortex center, a near solid-bodylike rotation in the viscous core of the vortex, and zero velocity at the center of the vortex (results in Fig. 6). Whereas a variety of mathematical models have been suggested for the spindown associated with the diffusion of tip vortices, one of the simplest is the classic Lamb–Oseen model (see Ref. 21). However, the Lamb–Oseen model is found to be unrealistically slow when compared to measurements. This is because of the laminar flow assumptions invoked in this model, that is, molecular diffusion only is allowed throughout the vortex. In light of experimental evidence, however, tip vortices are generally not entirely laminar, and so empirically modified Lamb–Oseen growth models are found to give better representations (see Ref. 11).

Bhagwat and Leishman[10,11] have modified the Squire model[7] with the inclusion of an average turbulent viscosity parameter δ to account for turbulence mixing on the net rate of diffusion, effectively increasing the viscous core growth rates to values that are more consistent with experimental observations. Furthermore, at $t = 0$, the swirl velocity given by the Lamb–Oseen model is singular at the origin of the tip vortex, and so unrealistically high velocities are then obtained at young wake ages compared to measurements. Therefore, an effective origin offset can be used to give the tip vortex a finite core size and finite induced velocity at its origin. Bhagwat and Leishman[10,11] suggest that the viscous core radius r_c of the tip vortices can be effectively modeled as a function of age ζ, using the equation

$$r_c(\zeta) = \sqrt{4\alpha\delta\nu[(\zeta - \zeta_0)/\Omega]} \equiv \sqrt{r_0^2 + 4\alpha\delta\nu\zeta/\Omega} \qquad (4)$$

where α is the Oseen constant and δ is the average turbulent diffusion parameter. The ordinate shift ζ_0 is responsible for the nonzero effective core radius r_0 at the tip vortex origin, where $\zeta = 0$ deg, to give a more physically correct (finite) induced velocity there compared to the Lamb–Oseen result.

Results from this diffusion model are shown in Fig. 7. Notice that the growth of the vortex core is relatively quick at young wake ages, but grows less slowly at older wake ages, which is generally consistent with experimental observations. The proper determination of δ and r_0 is clearly key to the success of this form of the model, and the determination of these parameters is considered later.

Modeling of Strain Effects

To understand the interdependent consequences of strain effects acting on a viscous vortex filament as it advects and diffuses inside the rotor wake, consider a linear section of an axisymmetric vortex filament of arbitrary length l and with the vorticity concentrated over a cross-sectional area S (Fig. 9). In the absence of external viscous effects, Helmholtz's laws require conservation of circulation Γ of the filament, which can be mathematically stated as

$$\Gamma = \int_S \boldsymbol{\omega} \cdot \mathrm{d}\boldsymbol{S} = \text{const} \qquad (5)$$

It has been shown in Fig. 8 that the measured circulation in the tip vortex decays only very slowly with wake age. Suppose after a time $t + \Delta t$, the filament advects to a new position under the influence of the local velocity field and it becomes strained, as shown in Fig. 9. Conservation of volume (constant density assumption) implies that the change in filament length is accompanied by a corresponding change in the cross-sectional area over which the vorticity is distributed. Therefore, a change in the filament length is accompanied by a proportional change in its vorticity; see also Saffman[4] and Leonard.[23] In cases where the strains are large, this can have a pronounced effect on the induced velocity field in the immediate vicinity of the vortex filament.

It can be assumed that the bulk of the vorticity is contained with the vortex core, although this depends to some extent on the assumption of a particular velocity profile. For a given self-similar vortex model, the change in the filament core radius resulting from the imposed strain is calculated using volume conservation, which gives

$$\Delta r_c = r_c\left[1 - \left(\sqrt{1+\varepsilon}\right)^{-1}\right] \qquad (6)$$

The result in Eq. (6) also satisfies momentum and energy conservation implicitly. Note that the preceding argument is strictly valid only in incompressible or constant density flowfields. In a fully compressible flow, the stretching of the filament need not necessarily be accompanied by an increase in vorticity because the density of the fluid will also change with filament stretching. The formation of rotor tip vortices clearly involve compressibility effects,[24] however, it is reasonable to assume that to a first level of approximation that any changes in flow density are small enough so that an increase in vorticity can be considered to be the primary effect of filament stretching. This is justified, at least, from the present experimental results.

Correction for Strain Effects

In light of the foregoing, it is apparent in a practical sense the mechanisms of viscous/turbulent diffusion and the effects of strain fields can act to change both the size and growth rate of the viscous core. In Fig. 10, the measured core growth results are plotted as a function of wake age. In this case, the results are now corrected to account for the effects of strain, assuming the validity of Eq. (6) and using the measured values of strain as given in Fig. 5. Notice that the correction makes a difference at older wake ages where the strain rates are large and that the results now fall into much better agreement with the overall trends resulting from diffusion alone, that is, without the effects of strain. The results suggest that an average value of $\delta = 8$ (in this case) gives good agreement with the measured results.

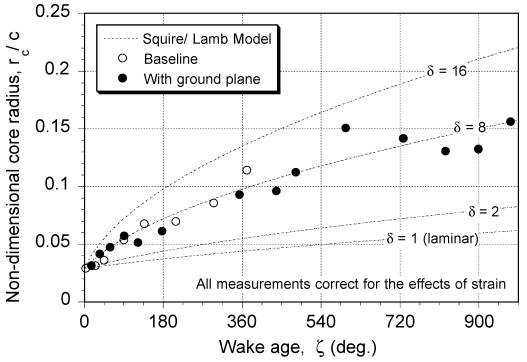

Fig. 10 Trends in the core growth when correcting the measurements for the effects of filament strain.

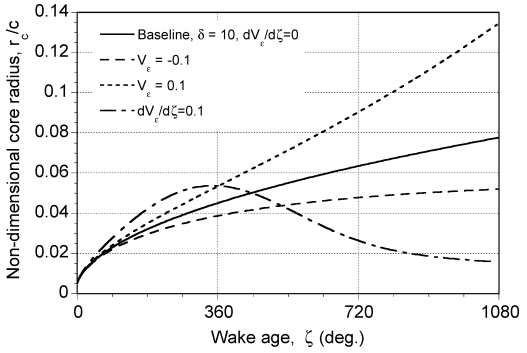

Fig. 11 Representative growth of the viscous core radius of a rectilinear vortex filament as a function of time (wake age) under the action of idealized strain rates.

Blade Tip Vortex Modeling

Combined Growth Model

The forgoing results suggest that a simple engineering tip vortex model can be developed that accounts for the combined and interdependent effects of viscous/turbulent diffusion and the effects of flowfield strain. When Eqs. (4) and (6) are used, the two equations can be combined to give an equation for the core growth as

$$r_c(\zeta, \varepsilon) = \sqrt{r_0^2 + \frac{4\alpha\delta\nu}{\Omega}\int_{\zeta_0}^{\zeta}(1+\varepsilon)^{-1}\,\mathrm{d}\zeta} \tag{7}$$

The strain rate ε can be determined based on a knowledge of the local velocity field in which the vortex develops; this would normally be calculated as part of the rotor wake model. The two empirical parameters in this model that are used to describe the viscous/turbulent diffusion are the initial core radius r_0 (or virtual time ζ_0) and the average turbulent diffusion parameter δ, which is known to depend on vortex Reynolds number.

The significance of strain effects using Eq. (7) can first be illustrated with reference to the development of a rectilinear vortex filament. The effects were examined for a prescribed strain rate, as defined by $V_\varepsilon = \mathrm{d}\varepsilon/\mathrm{d}t$. In the first instance, uniform strain rates were applied such that $V_\varepsilon(\zeta) = \text{const}$, and in the second instance, linear strain rates were applied such that $V_\varepsilon(\zeta) = A + (\mathrm{d}V_\varepsilon/\mathrm{d}\zeta)\zeta$ with the assumption of $A = -0.5$. This latter form is representative of the conditions found in hovering flight, where the wake initially contracts below the rotor (filaments squeezed) and then becomes constant or slowly starts to expand radially outward (filaments stretched) as the wake gets older and is advected into the downstream region (also Fig. 5). The results are compared to the baseline case where diffusion alone (with $\delta = 10$) is allowed in a zero strain field.

Notice in Fig. 11 that the effects obtained differ depending on whether the filament is stretched or squeezed with time. For negative strain rates, to conserve volume (conservation of mass, constant density flow) the core radius is found to increase rapidly compared to that obtained with positive strain. Furthermore, in this case the effects of diffusion and strain on the viscous core development act in a complementary manner. With positive strain rates, the core radius becomes nominally constant for later values of time. In this case, after an initial development, the increase in core radius resulting from diffusion can be balanced by the decrease in the core radius as a result of filament stretching. The results in Fig. 11 also illustrate an interesting consequence of imposing varying strain rates along the length of a vortex filament. In the baseline diffusion model (without strain rate effects), the cores of the filament at later wake ages are significantly larger than found with the applied strain rate. In other words, the segments of the wake undergoing positive strain or stretching may have a much smaller core radius, even though they have diffused in the flow for a longer time. This means that the peak induced swirl velocity surrounding those segments is larger and that the vorticity is more concentrated than that found at the earlier wake ages.

To further show the validity of the model in Eq. (7), it has been used to predict the core growth with the assumptions of $\delta = 8$ (Fig. 10) and using the measured (estimated) strain rates defined by the results in Fig. 5. The results are shown in Fig. 12, where it is apparent that the proposed engineering model faithfully predicts the measured core growth. Such levels of correlation give considerable confidence in the ability of this type of model to predict the viscous core growth for a rotor tip vortex encountering an arbitrarily imposed strain rate.

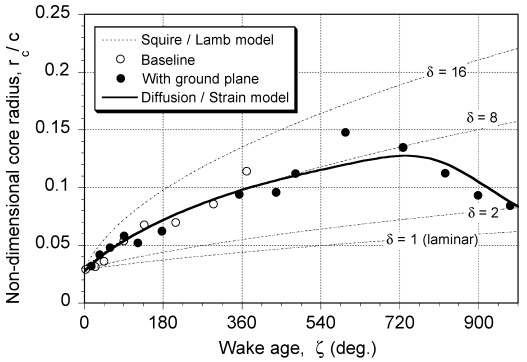

Fig. 12 Predictions of core growth under the assumptions of diffusion with $\delta = 8$ in a known strain field.

Model for δ

As already mentioned, the determination of the turbulent diffusion parameter δ is one key to the success of the proposed model. A purely laminar flow, that is, where diffusion of vorticity takes place on the molecular level alone, then $\delta = 1$. In such a case, with $\varepsilon = 0$ and $r_0 = 0$, then Eq. (7) reduces to the classical Lamb–Oseen core growth model. In most practical cases of lift-generated tip vortex flows, however, experimental measurements suggest that turbulence production increases the average rate of diffusion of vorticity so that $\delta > 1$, therefore, increasing the core growth rates. The details of this core growth process, however, are not fully understood, and existing experimental results are not entirely in agreement. There is evidence that the inner core growth is laminar and there is no turbulent mixing effects to enhance the diffusion of vorticity in this region.[20,25,26] There is also some evidence that turbulent flows surrounding the vortex core could undergo a process of relaminarization. Other measurements suggest that there is turbulence production at the edges of the laminar core,[27] which acts to increase the core growth.

Whereas complete understanding the details of tip vortex flows still requires much further research, for engineering models the more readily derived vortex properties such as the peak swirl velocity and effective core size can be used to better understand the overall vortex modeling requirements. Although the value of δ can be estimated from the present measurements, in the general case δ will be a function of vortex Reynolds number Re_v ($\equiv \Gamma_v/\nu$). For the present measurements, the vortex Reynolds number Re_v is of the order of 10^5. For a full-scale rotor, however, the values of vortex Reynolds number Re_v may be of the order of 10^7 or greater. Therefore, the

difficulty in constructing a more general tip, vortex model that has a wide range of applicability is to establish how δ will vary with vortex Reynolds number Re_v.

Functional Representation for δ

Squire[7] hypothesized that δ should be proportional to the vortex circulation strength. The value of δ was then formulated in terms of the vortex Reynolds number as

$$\delta = 1 + a_1 Re_v \tag{8}$$

where a_1 is a parameter that must be determined empirically from tip vortex measurements.

Most existing vortex models assume that the velocity profiles are self-similar, indicating that the vortex can be represented using a single shape function by appropriately scaling length scales and velocities.[11,20] Even when the profiles may not be self-similar, it is generally easier to measure the peak swirl velocity in the vortex flow than derived quantities such as its core dimension. Following an approach similar to Iversen[8] and Zeman,[9] Bhagwat and Leishman[10] have shown a correlation between the nondimensional peak swirl velocity and the wake age ζ or equivalent downstream distance d of the vortex. This correlation takes the form

$$\bar{V}_{\theta_{\max}} (\bar{d} + \bar{d}_0)^{\frac{1}{2}} = k \tag{9}$$

where the constants $\bar{d}_0$ and k can be determined empirically. In the case of a fixed wing, the non-dimensional velocity $\bar{V}_{\theta_{\max}}$ is defined as

$$\bar{V}_{\theta_{\max}} = \left(V_{\theta_{\max}} \big/ V_\infty\right)(V_\infty c/\Gamma_v) \tag{10}$$

and the equivalent nondimensional downstream distance $\bar{d}$ is defined as

$$\bar{d} = (z/c)(\Gamma_v/V_\infty c) \tag{11}$$

where z is the distance downstream of the wing. In the case of a rotating wing, the nondimensional velocity is defined as

$$\bar{V}_{\theta_{\max}} = \left(V_{\theta_{\max}} \big/ \Omega R\right)(\Omega R c/\Gamma_v) \tag{12}$$

and the equivalent nondimensional downstream distance is expressed in terms of wake age as

$$\bar{d} = \zeta \left(\Gamma_v \big/ \Omega c^2\right) \tag{13}$$

Examples of these Iversen-like correlation curves are shown for fixed-wing tip vortex measurements in Fig. 13 and for rotating wings in Fig. 14. Fixed-wing measurements have been taken from Refs. 28–35. For the rotating wings, measurements have been taken from Refs. 36–39. The measurements obtained in the present work were obtained at relatively old wake ages compared to that shown in other measurements and so can be used to further augment the correlation curves. In both cases (Figs. 13 and 14), the measurements

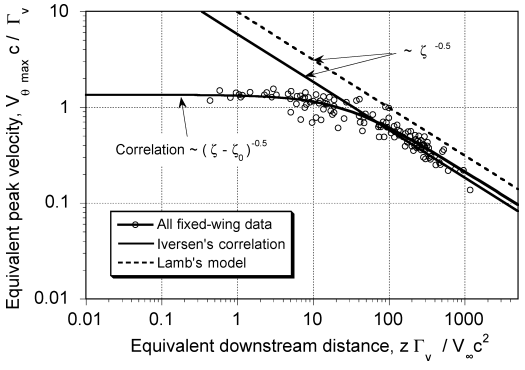

Fig. 13 Correlation of peak swirl velocity with equivalent downstream distance for fixed-wing tip vortex measurements.

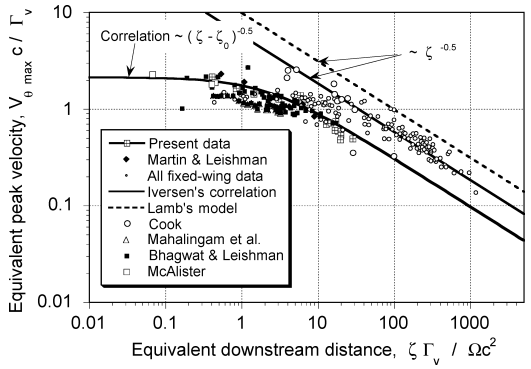

Fig. 14 Correlation of peak swirl velocity with equivalent downstream distance for helicopter rotor tip vortex measurements.

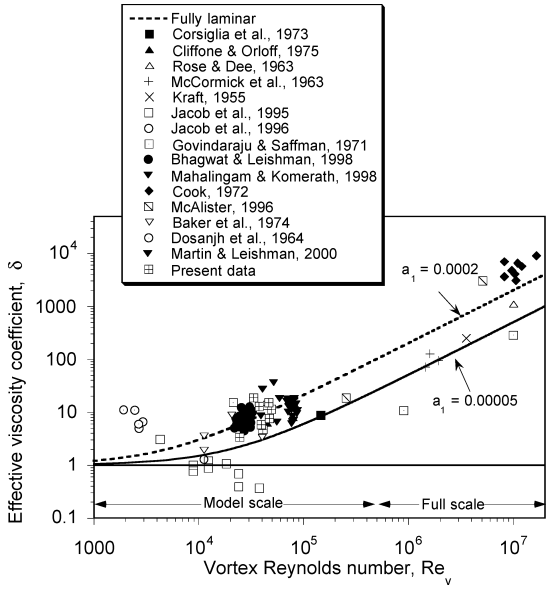

Fig. 15 Effective diffusion parameter δ as a function of vortex Reynolds number Re_v.

show a definitive trend as given by Eq. (9). With the transformation that $t = z/V_\infty$ (fixed wings) or $t = \zeta/\Omega$ (rotating wings), the correlation given by Eq. (9) shows that

$$V_{\theta_{\max}} \propto \sqrt{\Gamma_v/t} \tag{14}$$

The maximum swirl velocity as given by the Lamb–Oseen model is

$$V_{\theta_{\max}} \propto \Gamma_v/2\pi r_c \propto \Gamma_v \big/ \sqrt{\delta \nu t} \tag{15}$$

Therefore,

$$V_{\theta_{\max}} \propto \sqrt{\Gamma_v/t}\sqrt{(1/\delta)(\Gamma_v/\nu)} \tag{16}$$

When Eqs. (14) and (16) are compared, it follows that

$$(1/\delta)(\Gamma_v/\nu) = Re_v/\delta = \text{const} \tag{17}$$

which means that the average apparent viscosity coefficient δ is proportional to the vortex Reynolds number, Γ_v/ν. Therefore, this analysis supports the hypothesis that

$$\delta = 1 + a_1 Re_v \tag{18}$$

Determination of δ and a_1

Figure 15 shows an assemblage of tip vortex measurements (from the sources cited earlier) as the estimated value of δ from the measured core growth results, which is then plotted vs the corresponding vortex Reynolds number. The measured data include results

from fixed-wing as well as rotating-wing trailing vortices. Lines are shown for the predominantly laminar trend, that is, the Lamb–Oseen model, along with the trends obtained on the basis of Squire's hypothesis.

For low Reynolds numbers, the measurements show small and nominally constant values of δ, suggesting that the core is mostly laminar for these low Reynolds numbers. However, it is apparent that δ increases with increasing Reynolds number, with an almost linearly increasing trend at higher Reynolds numbers. Notice that any experimental values of $\delta < 1$ are physically impossible, and the various challenges and uncertainties in experimental measurements in making such measurements may account for such inconsistencies. The overall experimental evidence, however, strongly suggests the validity of Squire's hypothesis that enhanced turbulent diffusion of the vorticity from within the vortex core is directly proportional to the vortex Reynolds number.

Figure 16 shows the same experimental data in the form of Squire's parameter, a_1. The experimental data suggest that a_1 falls into the range $\mathcal{O}(10^{-3})$–$\mathcal{O}(10^{-4})$. However, it appears that the rotating-wing results show a slightly higher effective diffusion rate corresponding to an average value of $a_1 = \mathcal{O}(10^{-4})$, whereas the fixed-wing results show a lower value of $a_1 = \mathcal{O}(10^{-5})$. Note, however, that compared to fixed-wing vortex measurements most rotating-wing results will have the implicit effects of vortex straining resulting from filament curvature and other wake distortion effects included implicitly in the measurements, which may account for part of these differences. Unfortunately, it seems impossible to isolate and correct for these effects. Furthermore, isolating and correcting for the effects of wandering and aperiodicity (Appendix) in some of these measurements must be accomplished. This may be difficult or impossible in most experiments because the necessary statistics have simply not been measured. Clearly, however, the average value of a_1 is of the order of 10^{-3}–10^{-5} for all of the data shown here.

Combined Core Growth Model

Therefore, on the basis of the foregoing results and discussion, the equation

$$r_c(\zeta, \varepsilon) = \sqrt{r_0^2 + \frac{4\alpha\delta(Re_v)\nu}{\Omega}\int_{\zeta_0}^{\zeta}[1+\varepsilon(\zeta)]^{-1}\,\mathrm{d}\zeta} \qquad (19)$$

with $\delta(Re_v) = 1 + a_1 Re_v$ and $\varepsilon(\zeta)$ being equal to the local strain rate provides one type of engineering model for the growth of the viscous core of a trailing tip vortex under the action of both diffusion and stretching. For full-scale helicopter rotors, which will have tip vortices with much larger values of vortex Reynolds number Re_v, the correlation curve in Fig. 16 would suggest values of $\delta \approx 1000$. This suggests that a helicopter rotor tip vortex may exhibit turbulent diffusive characteristics that are orders of magnitude larger than compared to those expected on the basis of laminar diffusion alone.

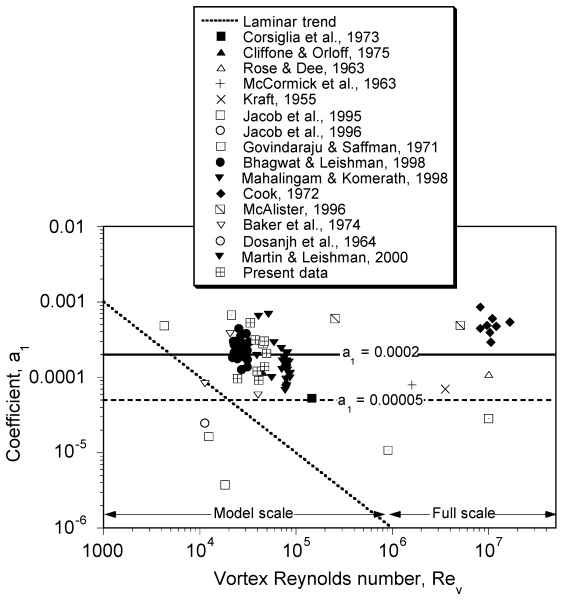

Fig. 16 Effective viscosity parameter, a_1, as a function of vortex Reynolds number, Re_v.

Finally, some estimate for the initial core radius r_0 is in order. The initial core radius of trailing vortices has been measured to be typically of the order if 5–10% of chord, that is, of the order of the airfoil thickness at the blade tip where the vortex originated. The effective origin offset, z_0 or ζ_0, can then be established from the initial core radius r_0 by using Eq. (4) or Eq. (7). It would seem that, from the data shown here, ζ_0 is on average between 20 and 25 deg.

Conclusions

An idealized experiment was performed to examine and quantify the interdependence of straining and diffusion on the tip vortices in a rotor wake flow. The properties of the blade tip vortices were measured in the wake of a small-scale hovering rotor and compared to the results for the case when the tip vortex was strained in a known velocity gradient. The results have been used in conjunction with other vortex measurements, to construct a more general engineering model for the vortex core growth that accounts for both the effects of diffusion and straining. The following conclusions have been drawn from the study.

1) The use of a ground plane was found to be successful in imposing a significant strain field on the developing rotor wake. This boundary created velocity gradients and forced the blade tip vortices to stretch, thus, allowing the effects of this stetching on the tip vortex development to be measured. From the measured displacements, the strain field was then estimated.

2) It was shown that vortex stretching slows the normal diffusive growth of the vortex core. When the strain rates become large, the effects can balance or counter the growth in the vortex core resulting from diffusion alone. A simple engineering model for the effects of diffusion and stretching was used to correct the measurements, which brought the results into remarkable agreement with what would be expected on the basis of diffusion alone.

3) As a byproduct of the process of stretching the tip vortex filaments, their properties could be measured to much older wake ages than would otherwise have been possible. Corrected results for zero strain field were used to compare with various other tip vortex measurements and to augment earlier correlations where measurements could not be made to such old wake ages, that is, for more than about $1\frac{1}{2}$ rotor revolutions.

4) The new results obtained here were used to help validate a more general core growth model that is suitable use in a variety of helicopter rotor aeroacoustic applications. The model combines the effects of turbulent diffusion and strain on the vortex core growth. The empirical coefficients of the model have been derived based on a compendium of available measurements documenting the viscous core growth of trailing vortices.

Appendix: Aperiodicity Correction

Aperiodicity is the inherent random movement of the phase-resolved spatial locations of the vortex cores inside the rotor wake. Measurements of aperiodicity were made using laser light-sheet illumination of the seeded flow. A laser pulse duration on the order of nanoseconds was achieved using an Nd:YAG laser. The laser was synchronized to the rotor so that the aperiodicity of the core position could be measured at a fixed wake age. A CCD camera with a microlens acquired the images, which were digitized and the vortex positions quantified with respect to a calibration grid. Various methods have been proposed for correcting measurements for aperiodicity or wandering.[40–43] The method of Leishman[42] is used here and accounts for an arbitrary velocity distribution and anisotropic variations in aperiodicity.

Consider the two-dimensional aperiodic motion of a tip vortex at a given wake age ζ. Define the LDV measurement location, which is fixed with respect to the rotor axes system, as (r_p, z_p). The current location of the vortex core axis relative to a rotor-based axis system is assumed to be (r_v, z_v). The velocity field measured at (r_p, z_p) at a wake age ζ will be functions of r and z and the position of the measurement point relative to an axis at the center of the vortex, that is,

$$V(r, z, \zeta) = V(r_p - r_v, z_p - z_v, \zeta) \tag{A1}$$

Over a sufficiently large number of rotor revolutions, the aperiodicity of the vortex location relative to the measurement point can be described by using a probability density function (PDF), for example, $p = p(r_v, z_v, \zeta)$. Following Devenport et al.,[41] it may be initially assumed that the aperiodicity is normal (Gaussian) so that a joint normal PDF can be defined as

$$p(r_p, z_p, \zeta) = \frac{1}{2\pi\sigma_r\sigma_z\sqrt{1-e^2}} \times \exp\left[\frac{-1}{2(1-e^2)}\left(\frac{r_v^2}{\sigma_r^2} + \frac{z_v^2}{\sigma_z^2} - \frac{2er_vz_v}{\sigma_r\sigma_z}\right)\right] \tag{A2}$$

where $\sigma_r = \sigma_r(\zeta)$ and $\sigma_z = \sigma_z(\zeta)$ are the measured rms. aperiodicity amplitudes in the radial and axial directions at each wake age, respectively, and $e = e(\zeta)$ is the correlation coefficient. When Eq. (21) is used, the actual or measured velocity $\bar{V}(r_p, z_p, \zeta)$ can then be determined by convolution, where

$$\bar{V}(r_p, z_p, \zeta) = \int^{\infty} \int_{-\infty} V(r_p - r_v, z_p - z_v, \zeta)\, p(r_v, z_v)\, \mathrm{d}r_v\, \mathrm{d}z_v \tag{A3}$$

The discrete equivalent of Eq. (22) is

$$\bar{V}(r_p, z_p, \zeta) = \sum\sum V(r_p - r_v, z_p - z_v, \zeta)\, p(r_v, z_v) \Delta r_v \Delta z_v \tag{A4}$$

This latter equation is solved by reexpressing V in a Cartesian coordinate system, and the summations are taken over length scales that are at least one order of magnitude larger than σ. An advantage of the numerical solution using Eq. (A4) is that very general velocity profiles such as the nonaxisymmetric tangential profiles generally found in rotor wakes can be solved to establish actual quantitative effects of aperiodicity on the results.

Starting from an initial (assumed) tangential velocity profile without any aperiodicity, a profile with the effects of aperiodicity can be obtained numerically by using Eq. (A4). Then a correction can be applied and a new guess made at the true tangential velocity. The process can be repeated using Eq. (A4) until convergence is obtained, which is typically within a few iterations, yielding an estimate of the true velocity field based on the measured velocity field.

Acknowledgments

The authors wish to thank Mahendra Bhagwat and Shreyas Ananthan for their contributions to this work. This research was supported, in part, by the National Rotorcraft Technology Center under Grant NCC 2944. Yung Yu and Thomas Doligalski were the Technical Monitors.

References

[1]Schmitz, F. H., "Rotor Noise," *Aeroacoustics of Flight Vehicles: Theory and Practice*, Vol. 1, NASA Reference Publ. 1258, 1991, Chap. 2.

[2]Martin, P. B., Pugliese, G. J., and Leishman, J. G., "Laser Doppler Velocimetry Uncertainty Analysis for Rotor Blade Tip Vortex Measurements," *38th Aerospace Sciences Meeting and Exhibit*, AIAA Paper 2000-0263, Reston, VA, 2000.

[3]Leishman, J. G., and Bagai, A., "Challenges in Understanding the Vortex Dynamics of Helicopter Rotor Wakes," *AIAA Journal*, Vol. 36, No. 7, 1998, pp. 1130–1140.

[4]Saffman, P. G., *Vortex Dynamics*, Cambridge Univ. Press, Cambridge, England, U.K., 1992, Chap. 1.

[5]Carrier, G. F., Fendell, F. E., and Marble, F. E., "Effect of Strain Rate on Diffusion in Flames," *SIAM Journal on Applied Mathematics*, Vol. 28, No. 2, 1975, pp. 463–500.

[6]Ananthan, S., Leishman, J. G., and Ramasamy, M., "The Role of Filament Stretching in the Free-Vortex Modeling of Rotor Wakes," American Helicopter Society 58th Annual National Forum, 11–13 June 2002.

[7]Squire, H. B., "The Growth of a Vortex In Turbulent Flow," *Aeronautical Quarterly*, Vol. 16, Aug. 1965, pp. 302–306.

[8]Iversen, J. D., "Correlation of Turbulent Trailing Vortex Decay Data," *Journal of Aircraft*, Vol. 13, No. 5, 1976, pp. 338–342.

[9]Zeman, O., "The Persistence of Trailing Vortices: A Modeling Study," *Physics of Fluids*, Vol. 7, No. 1, 1995, pp. 135–143.

[10]Bhagwat, M. J., and Leishman, J. G., "Correlation of Helicopter Tip Vortex Measurements," *AIAA Journal*, Vol. 38, No. 2, 2000, pp. 301–308.

[11]Bhagwat, M. J., and Leishman, J. G., "Viscous Vortex Core Models for Free-VortexWake Calculations," Proceedings of the 58th Annual Forum of the American Helicopter Society International, 11–13, June 2002.

[12]Bir, G., Chopra, I., and Nguyen, K., "Development of UMARC (University of Maryland Advanced Rotor Code)," Procedings of the 46th Annual Forum of the American Helicopter Society, Washington D.C., May 1990.

[13]Johnson, W., "CAMRAD II, Comprehensive Analytical Model of Rotorcraft Aerodynamics and Dynamics," Johnson Aeronautics, Palo Alto, CA, 1992–1997.

[14]Stephens, W. B., Rutkowski, M. J., Ormiston, R. A., and Tan, C. M., "Development of the Second Generation Comprehensive Helicopter Analysis System (2GCHAS)," American Helicopter Society National Technical Specialists Meeting on Rotorcraft Dynamics, Nov. 1989.

[15]Martin, P. B., Bhagwat, M. J., and Leishman, J. G., "Strobed Laser Sheet Visualization of a Helicopter Rotor Wake," *Journal of Flow Visualization and Image Processing*, Vol. 7, No. 1, 1999, pp. 31–50.

[16]Bhagwat, M. J., and Leishman, J. G., "Stability Analysis of RotorWakes in Axial Flight," *Journal of the American Helicopter Society*, Vol. 45, No. 3, 2000, pp. 165–178.

[17]Light, J. S., and Norman, T., "Tip Vortex Geometry of a Hovering Helicopter Rotor in Ground Effect," 45th Annual Forum of the American Helicopter Society, 22–24, May 1989.

[18]Leishman, J. G., "Seed Particle Dynamics in Tip Vortex Flows," *Journal of Aircraft*, Vol. 33, No. 4, 1996, pp. 823–825.

[19]Barrett, R. V., and Swales, C., "Realisation of the Full Potential of the Laser Doppler Anemometer in the Analysis of Complex Flows," *Aeronautical Journal*, Vol. 102, No. 1016, 1998, pp. 313–320.

[20]Martin, P. B., Pugliese, G., and Leishman, J. G., "High Resolution Trailing Vortex Measurements in the Wake of a Hovering Rotor," *Journal of the American Helicopter Society*, Vol. 48, No. 1, 2003, pp. 39–52.

[21]Lamb, H., *Hydrodynamics*, 6th ed., Cambridge University Press, Cambridge, England, U.K., 1932.

[22]Oseen, C. W., "UberWirbelbewegung in Einer Reibenden Flussigkeit," *Ark. J. Mat. Astrom. Fys*., Vol. 7, 1912, pp. 14–21.

[23]Leonard, A., "Vortex Methods for Flow Simulation," *Journal of Computational Physics*, Vol. 37, No. 3, Oct. 1980, pp. 289–335.

[24]Bagai, A., and Leishman, J. G., "Flow Visualization of Compressible Vortex Structures Using Density Gradient Techniques," *Experiments in Fluids*, Vol. 15, No. 6, 1993, pp. 431–442.

[25]Cotel, A. J., and Breidenthal, R. E., "Turbulence Inside a Vortex," *Physics of Fluids*, Vol. 11, No. 10, 1999, pp. 3026–3029.

[26]Cotel, A. J., "Turbulence Inside a Vortex: Take Two" *Physics of Fluids*, Vol. 14, No. 8, 2002, pp. 2933–2934.

[27]Han, Y. O., Leishman, J. G., and Coyne, A. J., "On the Turbulent Structure of a Tip Vortex Generated by a Rotor," *AIAA Journal*, Vol. 35, No. 3, 1997, pp. 477–485.

[28]Govindraju, S. P., and Saffman, P. G., "Flow in a Turbulent Trailing Vortex," *Physics of Fluids*, Vol. 14, No. 10, 1971, pp. 2074–2080.

[29]Jacob, J., Savas, O., and Liepmann, D., "Trailing Vortex Wake Growth Characteristics of a High Aspect Ratio Rectangular Airfoil," *AIAA Journal*, Vol. 35, No. 2, 1997, pp. 275–280.

[30]Jacob, J., Savas, O., and Liepmann, D., "Experimental Investigation of Forced Wake Vortices on a Rectangular Wing," AIAA Paper 96-2497, June 1996.

[31]Ciffone, D. L., and Orloff, K. L., "Far-Field Wake-Vortex Characteristics of Wings," *Journal of Aircraft*, Vol. 12, No. 5, 1975, pp. 464–470.

[32]Corsiglia, V. R., Schwind, R. G., and Chigier, N. A., "Rapid Scanning, Three Dimensional Hot Wire Anemometer Surveys of Wing-Tip Vortices," NASA CR-2180, July 1973.

[33]McCormick, B. W., Tangler, J. L., and Sherrieb, H. E., "Structure of Trailing Vortices," *Journal of Aircraft*, Vol. 5, No. 3, 1968, pp. 260–267.

[34]Kraft, C. C., "Flight Measurements of the Velocity Distribution and Persistence of the Trailing Vortices of an Airplane," NACA TN 3377, March 1955.

[35]Rose, R., and Dee, W. F., "Aircraft Vortex Wake and Their Effects on Aircraft," Aeronautical Research Council, Rept. CP-795, London, Dec. 1965.

[36]Bhagwat, M. J., and Leishman, J. G., "Measurements of Bound and Wake Circulation on a Helicopter Rotor," *Journal of Aircraft*, Vol. 37, No. 2, 2000, pp. 227–234.

[37]Mahalingam, R., and Komerath, N. M., "Measurements of the Near Wake of a Rotor in Forward Flight," AIAA Paper 98-0692, Jan. 1998.

[38]Cook, C. V., "The Structure of the Rotor Blade Tip Vortex," *Aerodynamics of Rotary Wings*, CP-111, AGARD, 1972, pp. 14–27.

[39]McAlister, K. W., "Measurements in the NearWake of a Hovering Rotor," AIAA Paper 96-1958, June 1996.

[40]Heineck, J. T., Yamauchi, G. K., Wadcock, A. J., and Lourenco, L., "Application of Three-Component PIV to a Hovering Rotor Wake," 56th Forum of the American Helicopter Society, May, 2000.

[41]Devenport, W. J., Rife, M. C., Liapis, S. I., and Follin, G. J., "The Structure and Development of a Wing-tip Vortex," *Journal of Fluid Mechanics*, Vol. 312, 1996, pp. 67–106.

[42]Leishman, J. G., "Measurements of the Aperiodic Wake of a Hovering Rotor," *Experiments in Fluids*, Vol. 25, No. 4, Sept. 1998, pp. 352–361.

[43]Gursul, I., and Xie, W., "Origin of Vortex Wandering Over Delta Wings," *Journal of Aircraft*, Vol. 37, No. 2, 1999, pp. 348–350.